Systematic modeling study of channel waveguide fabrication by thermal silver ion exchange

Guangyu Li, Kim A. Winick, Henry C. Griffin, and Joseph S. Hayden

A systematic study of thermal silver ion exchange used for the fabrication of optical channel waveguides is reported in a single-alkali glass. The diffusion equilibrium and diffusion dynamics are experimentally studied, and the concentration-dependent diffusion coefficients are determined. The relationship between the fabrication conditions, i.e., time, temperature, and melt concentration, and the induced waveguide refractive index profile is established. It is demonstrated that the diffusion equation can be solved, without use of any free parameters, to predict the refractive index profiles of both planar and channel waveguides. A 1.6 cm diameter integrated optic ring resonator, with a propagation loss of 0.1 dB/cm, is fabricated in a glass by thermal silver ion exchange. The induced refractive index profile is related to the optical characteristics of the functional device.   © 2006 Optical Society of America

OCIS codes: 130.2790, 130.3130, 230.3120, 230.7380, 230.7390.

1.   Introduction

Ion exchange is a widely used technology for the fabrication of both passive and active glass integrated optical devices. It has a number of advantages, including simplicity, low cost, and optical fiber compatibility. The first integrated optic waveguide was fabricated by ion exchange in 1972,[1] and a large number of studies and review articles on ion exchange in glass have been published in the intervening years.[2–5] These studies generally fall into one of two categories: (1) those that investigate the physical chemistry of the ion exchange process[6–11] and (2) those that model waveguide fabrication for device applications.[12–35] The studies of the first kind investigate only the one-dimensional (1-D) indiffused ion concentrations and fail to connect these results with the induced refractive index profiles in channel waveguides. Studies of the second kind often invoke simplifying assumptions of questionable validity. These assumptions include any or all of the follow-ing: (a) the concentration of the indiffused ion in the glass is very low, (b) the self-diffusion coefficients are concentration independent, and (c) only a single pair of alkali species is involved in the exchange process even when the virgin glass contains multialkali species. In addition, for studies of the second kind, the diffusion coefficients are often assumed to be free parameters of the model, and these coefficients are indirectly inferred from the measured effective indices of the resulting waveguide modes. Comparisons of the diffusion coefficients obtained in this manner with those obtained by a more direct measurement are generally lacking. Finally, the quantitative modeling results that have been reported to date, which do not invoke any of these simplifying assumptions, have been performed for planar rather than the more important class of channel waveguides.[32]

In this paper, these deficiencies are rectified for the thermal silver ion exchange process. In particular, in Section 2 the concentration-dependent self-diffusion and interdiffusion coefficients are directly measured in a single-alkali glass. The relationship between the induced refractive index change and the indiffused silver ion concentration is also established together with its wavelength dependence. Using this data, the Fickian diffusion equation is solved numerically in Section 3 to determine the indiffused silver ion concentration. These data are applied for the first time, to the best of our knowledge, to predict the induced refractive index profiles of both planar and channel waveguides that are fabricated under a variety of conditions. These predictions are compared with the

G. Li (guangyul@umich.edu) and K. A. Winick are with the Department of Electrical Engineering and Computer Science, University of Michigan, 1301 Beal Avenue, Ann Arbor, Michigan 48109. H. C. Griffin is with the Department of Chemistry, University of Michigan, 930 North University Avenue, Ann Arbor, Michigan 48109. J. S. Hayden is with Schott North America, Incorporated, Regional Research and Development, 400 York Avenue, Duryea, Pennsylvania 18642.

measured profiles. The agreement is excellent for planar waveguides and reasonably good for channels. In Section 4 we relate the induced refractive index profile, produced by thermal silver ion exchange, to the optical characteristics of a functional device. A series of low-loss integrated optic ring resonators are fabricated, each of which contains a directional coupler. Using measured waveguide refractive index profiles, the crossover efficiencies of these couplers are calculated by coupled-mode theory (CMT), and the results are shown to be in excellent agreement with measurements. Finally in Section 5 our results are summarized.

2. Ion Exchange Modeling

We consider only ion exchange from a liquid melt in the absence of an externally applied electric field. Under such conditions, it is common to exchange sodium cations (Na^+) in the glass with either silver cations (Ag^+) or potassium cations (K^+) from the melt, although other ions have also been investigated.[2–5] In the silver ion exchange process studied here, Ag^+ ions are introduced into the glass at an elevated temperature by a $AgNO_3$:$NaNO_3$ molten salt bath that lies in diffusive contact with the glass surface. Na^+ cations in the glass are replaced by Ag^+ cations from the melt as these cations pass through lithographically patterned mask openings on the glass surface. The ion exchange process locally modifies the Ag^+ and Na^+ concentrations inside the glass, thus inducing local refractive index changes. The induced changes are a function of the ion exchange conditions, i.e., melt concentration, diffusion temperature, diffusion time, and the geometry of the mask openings.

Ag^+ ion exchange has several advantages relative to K^+ ion exchange, including lower processing temperatures, shorter exchange times, larger achievable refractive index changes, and the absence of stress-induced birefringence.[2,36,37] Silver ion exchange, however, requires proper glass selection to achieve a very low propagation loss and mode compatibility with standard optical fiber.

In the remainder of this section, glass selection and the ion exchange modeling procedure will be described in detail.

A. Glass Selection

Glass substrates, such as BK7 and Corning 0211, which are often used for ion exchange, generally contain more than one alkali oxide component, with Na_2O and K_2O being common constituents.[2] In mixed-alkali glasses each of the alkali elements will simultaneously participate in the ion exchange process. In most silver ion exchange waveguide modeling papers, the effects of these nonsodium alkali glass constituents are neglected without justification. In addition, when potassium is present, it will outdiffuse into the melt-inducing stresses in the glass. These stresses, in turn, can produce microcracks on the glass surface that are readily observable under a microscope.[36]

Table 1. Glass Composition

Oxide	IOG10 (wt. %)	IEG (wt. %)
SiO_2	63.6	64.0
Na_2O	9.2	12.0
K_2O	6.8	—
Al_2O_3	3.0	2.8
MgO	2.8	2.8
ZnO	12.5	15.6
B_2O_3	1.0	1.0
TiO_2	0.6	0.6
Traces	0.5	1.2

For the specific purpose of ion exchange modeling, a small batch of a single-alkali (Na_2O) ion-exchangeable silicate glass, hereafter referred to as IEG, was melted. A compositional analysis of IEG and a commercially available ion-exchangeable glass, Schott IOG10, was obtained through an outside service. The analysis was performed using x-ray fluorescence, inductively coupled plasma, and atomic absorption spectroscopy. The results of this analysis are shown in Table 1.

The nonbridging oxygen (NBO) content of a glass is an important factor in the selection of a substrate for silver ion exchange. It is known that the presence of NBOs causes reduction of silver ions and the subsequent formation of metallic silver clusters during silver ion exchange.[38] These metallic clusters discolor the glass and increase propagation losses in waveguide devices. The NBO content of both IEG and IOG10 were determined using x-ray photoelectron spectroscopy (XPS).[39] The XPS signal consists of two Gaussian-shaped signal components centered at the respective binding energies (i.e., 532.5 and 531 eV) of the bridging oxygens (BOs) and NBOs. The number of BOs and NBOs are directly proportional to the areas under the respective Gaussian-shaped component curves. The XPS signal along with the BO and NBO Gaussian component fits for IEG are shown in Fig. 1, and the NBO content is tabulated in Table 2. The lower NBO content of IEG is consistent with our
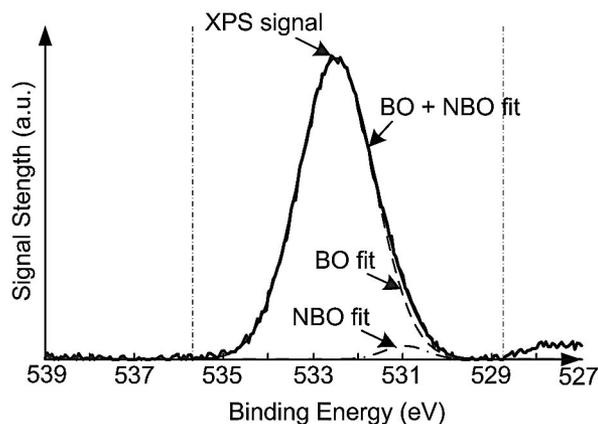

Fig. 1. XPS-measured oxygen spectrum of IEG. Gaussian fits give the BO and NBO contents.

Table 2. X-Ray Photoelectron Spectroscopy Results for Nonbridging Oxygen Analysis

Glass Substrate	NBO Fraction of Total Oxygens (%)
IOG10	10
IEG	2

observations that IOG10 suffers some yellow discoloration following silver ion exchange, especially at high silver melt concentrations, whereas IEG does not (even at $AgNO_3$ concentrations approaching 90 mol.%).

B. Ion Exchange Equilibrium at the Melt–Glass Interface

The ion concentrations at the interface between the glass sample and the melt were investigated at equilibrium. This investigation established the relationship between the silver ion concentration in the melt and the silver concentration immediately inside the glass surface. Similar studies have been previously reported in a variety of glasses.[6] When the chemical reaction at the melt–glass interface reaches equilibrium, the ions are distributed between the two phases (i.e., melt and glass) in a fixed ratio as described by[6]

$$\ln\left(\frac{m_{Ag}}{m_{Na}}\right) - \frac{E}{RT}(1 - 2m_{Na}) = n\ln\left(\frac{c_{Ag}}{c_{Na}}\right) - \ln K, \quad (1)$$

where K and n are thermodynamic constants that depend on the glass composition; E is the net interaction energy that is equal to 3.5 kJ/mol for silver nitrate–sodium nitrate salt melts[40]; R is the gas constant; T is the absolute temperature; m_{Ag} and m_{Na} are the mole fractions of $AgNO_3$ and $NaNO_3$ in the melt; and c_{Ag} and c_{Na} are the relative concentrations of Ag and Na ions, respectively, in the glass, i.e., $c_{Ag(Na)}$ = [number of Ag (Na) atoms in the glass]/(total number of Ag and Na atoms in the glass). Once the values of n and K are established, the silver ion concentration immediately inside the glass surface at equilibrium may be computed from knowledge of the $AgNO_3$ concentration in the melt.

The experimental study of the melt–glass interface equilibrium for IEG was carried out by performing ion exchanges at 320 °C using a $AgNO_3$:$NaNO_3$ melt mixture whose concentration was varied over a range from 0.2 to 90 mol.% $AgNO_3$. The exchange times were sufficiently long (i.e., 9 h) to ensure that a surface layer of the glass with a thickness of least several micrometers reached equilibrium with the melt. A 0.5 μm thick surface layer of the glass sample was chemically removed using diluted hydrofluoric acid. The ratio of silver-to-sodium atom concentration in the etchant, c_{Ag}/c_{Na}, was determined using an atomic absorption spectrophotometer. The unknown parameters for n and K appearing in Eq. (1) were fit to this measured data, yielding values of 1.27 and 46 for n and K, respectively, as shown in Fig. 2.
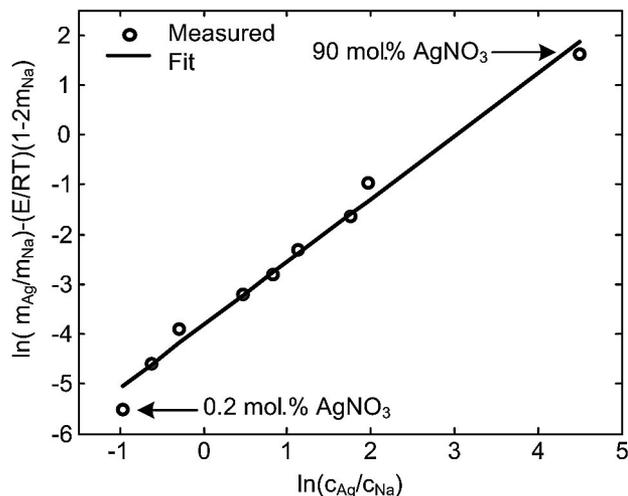

Fig. 2. Ion exchange equilibrium study at 320 °C in IEG.

Note that even melts having low $AgNO_3$ concentrations can produce large relative Ag concentrations inside IEG at equilibrium. For example, Fig. 2 indicates that a 1 mol.% $AgNO_3$ and 99 mol.% $NaNO_3$ melt corresponds to $c_{Ag} = 0.5$ at 320 °C.

Next, the silver ion concentration was related to the induced refractive index change. The surface refractive index change Δn_{surf} of silver ion-exchanged IEG samples was measured at a wavelength of 658 nm using a commercial refractive near-field (RNF) profilometer.[41] The results of these measurements are plotted versus melt concentration in Fig. 3. Combining the data shown in Figs. 2 and 3, a linear dependence between the surface refractive index change Δn_{surf} and the surface silver concentration immediately inside the glass surface $c_{Ag}(0)$ was established. This linear relationship is shown in Fig. 4. Two other independent methods, energy dispersive x-ray (EDX) and backscattered electron (BSE), using a scanning electron microscope were also used to compare the normalized silver concentration profile $c_{Ag}(x)/c_{Ag}(0)$ with
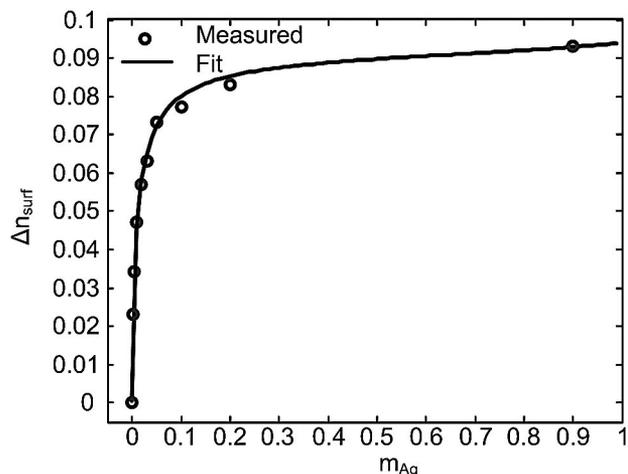

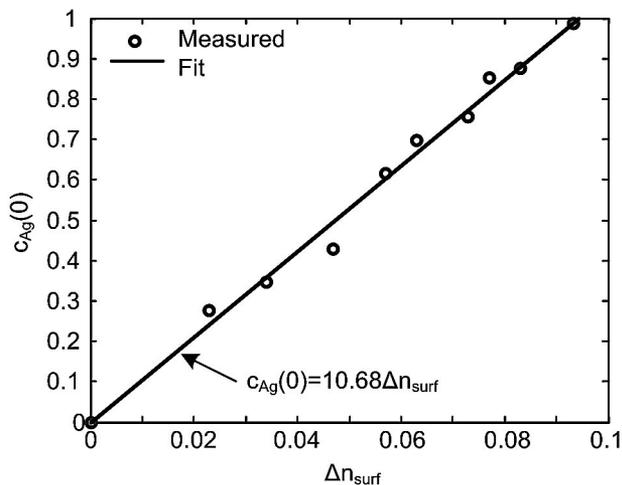Fig. 3. Surface index change in IEG at 658 nm versus mole fraction of $AgNO_3$ in the melt at 320 °C.

Fig. 4. Linear dependence of surface index change (Δn_{surf}) at 658 nm with the silver concentration at the glass surface [$c_{Ag}(0)$].

the normalized refractive index change profile $\Delta n(x)/\Delta n_{surf}$ measured by a RNF profilometer, where x denotes the depth inside the glass surface. All three of these measurement techniques yielded consistent results as illustrated in Fig. 5 for a 9 h exchange at 320 °C using a 10 mol.% silver nitrate melt.

C. Diffusion Dynamics

The kinetics of the thermal ion exchange process can be described by Fickian diffusion theory,[2–9] which states that the flux of ions crossing any plane will be proportional to the concentration gradient measured across that plane. Therefore the Ag⁺ cation concentration C_{Ag} in the glass is determined by Fick's first law:

$$\frac{\partial C_{Ag}}{\partial t} = \nabla \cdot (\tilde{D} \nabla C_{Ag}), \tag{2}$$

along with the appropriate boundary conditions. C_{Ag} is a function of both position and time, and $\tilde{D}$, the interdiffusion coefficient, is generally concentration

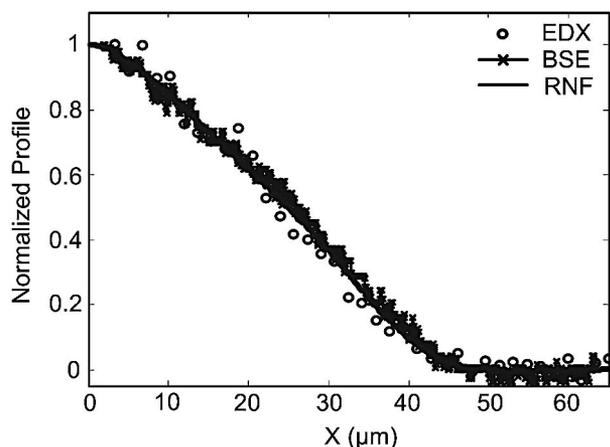dependent. Invoking the assumption of local charge neutrality, the concentration of the Na⁺ cation, C_{Na}, in the glass is given by

$$C_{Na} = C_0 - C_{Ag}, \tag{3}$$

where C_0 is the Na concentration in the virgin glass before ion exchange. We will find it more convenient to work with the following relative concentrations:

$$c_{Ag} \equiv \frac{C_{Ag}}{C_0}, \ c_{Na} \equiv \frac{C_{Na}}{C_0}. \tag{4}$$

Once $\tilde{D}$ is known and the appropriate boundary conditions are specified, Eq. (2) can be solved for the relative concentration profile $c_{Ag}(x, y, z, t)$. In the general case, closed-form solutions are not obtainable and numerical techniques must be invoked. Note that application of Eq. (2) does not require that the diffusion process be understood at an atomic level. In fact, it is not yet possible to derive the interdiffusion coefficient from knowledge of the glass structure alone. Models for $\tilde{D}$ have been derived based on thermodynamic principles, but these models have not been totally successful in predicting experimental results, as will be discussed in Subsection 2.D.

For the case of a 1-D thermal ion exchange of duration t_f into a thick glass substrate from an undepleted melt, the boundary and initial conditions become

$$\begin{cases} c_{Ag} = c_{Ag}(x = 0), \ x = 0, \ t > 0 \\ c_{Ag} = 0, \ x > 0, \ t = 0 \end{cases}. \tag{5}$$

$c_{Ag}(x = 0)$ is given by Eq. (1), and evidence indicates that the equilibrium at the glass–melt interface is quickly established during the ion exchange process. By making the change of variables

$$\eta \equiv \frac{x}{\sqrt{t}}, \tag{6}$$

Eqs. (2) and (5) can be rewritten as

$$-\frac{\eta}{2} \frac{dc_{Ag}}{d\eta} = \frac{d}{d\eta}\left(\tilde{D} \frac{dc_{Ag}}{d\eta}\right), \tag{7}$$

$$\begin{cases} c_{Ag} = c_{Ag} \ (x = 0), \ \eta = 0 \\ c_{Ag} = 0, \ \eta = \infty \end{cases}. \tag{8}$$

Canceling the factor of $d\eta$ on both sides of Eq. (7), integrating this equation from $c_{Ag} = 0$ (at $\eta = \infty$) to $c_{Ag} = c_{Ag}'$(at $\eta = \eta'$), and noting that $dc_{Ag}/d\eta = 0$ at $\eta = \infty$, we obtain

$$\tilde{D}(c_{Ag}') = -\frac{1}{2t_f} \frac{dx(c_{Ag})}{dc_{Ag}}\bigg|_{c_{Ag} = c_{Ag}'} \int_0^{c_{Ag}'} x(c_{Ag})dc_{Ag} \tag{9}$$

Fig. 5. Measured Ag⁺ and Δn diffusion profiles in IEG obtained by the EDX, BSE, and RNF methods for a 9 h exchange at 320 °C using a 10 mol.% silver nitrate melt.
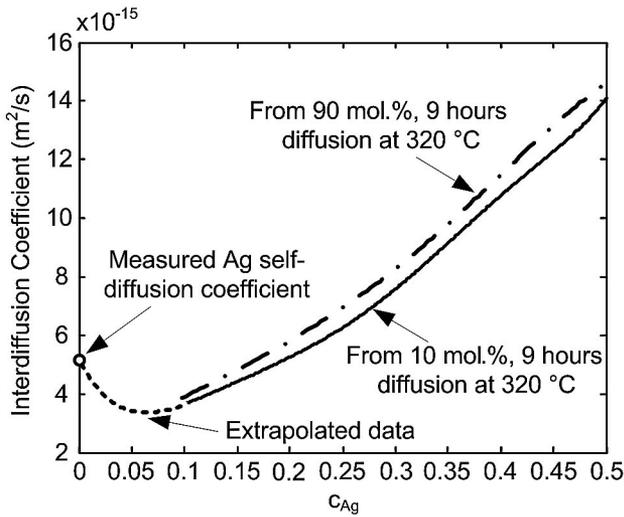
Fig. 6. Interdiffusion coefficient in IEG at 320 °C derived from a curve-fit RNF profile using the Boltzmann–Matano relation.

for $0 \leq c_{Ag}' \leq c_{Ag}(x = 0)$ provided that $c_{Ag}(x, t_f)$ is a monotonic function of x. Equation (9) is known as the Boltzmann–Matano relation.[42] This relation has been used extensively to recover concentration-dependent diffusion coefficients from measured concentration profiles.[32]

The Boltzmann–Matano inversion relation was applied to planar waveguides fabricated by a 9 h silver ion exchange at 320 °C using 10 mol.% AgNO$_3$:90 mol.% NaNO$_3$ and 90 mol.% AgNO$_3$:10 mol.% NaNO$_3$ salt mixtures. The 1-D refractive index profiles $\Delta n(x)$ were measured at 658 nm using a RNF profilometer, and $c_{Ag}(x)$ was computed from $\Delta n(x)$ using the linear relation established in Fig. 4. $\tilde{D}(c_{Ag})$ was subsequently computed using Eq. (9), and the results are displayed in Fig. 6 for c_{Ag} lying between 0.1 and 0.5 for both melt concentrations. As to be expected, the results do not depend on the melt concentration within the accuracy of our measurements.

The Boltzmann–Matano inversion method is sensitive to the shape of the concentration profile, especially near the glass surface (i.e., $x = 0$) where c_{Ag} is slowly changing (hence dx/dc_{Ag} is very large) and near the tail of the concentration profile where c_{Ag} is small. The measured concentration profile needs to be carefully curve fitted to reduce the effects of noisy experimental data before the Boltzmann–Matano inversion procedure is numerically implemented. The Ag concentration profile was fit using a ninth-order polynomial except in the tail region where exponential fitting was performed. Care had to be taken to ensure that the transition from the polynomial to the exponential fit regions occurred smoothly. The interdiffusion coefficient was obtained for c_{Ag} lying between 0 and 0.9. The data obtained by the Boltzmann–Matano procedure for c_{Ag} values greater than 0.5 or less than 0.1 are not shown in Fig. 6 because the flatness of the concentration profile near the glass surface and the low Ag concentration in the tails of the profile make the

inversion process quite sensitive to noisy data in these ranges.

At $c_{Ag} = 0$, the interdiffusion coefficient equals the silver self-diffusion coefficient, and this later value was measured and is reported in Subsection 2.D. The self-diffusion coefficient is shown in Fig. 6 and was used to extrapolate (dashed curve) the interdiffusion coefficient data obtained from the Boltzmann–Matano procedure down to $c_{Ag} = 0$.

D. Self-Diffusion Coefficients

By invoking a number of assumptions, the functional form of the interdiffusion coefficient may be determined.[4] The chemical potential of cation species i may be written as[8]

$$\varepsilon_i = \varepsilon_i{}^{(0)} + RT \ln(\gamma_i C_0 c_i V_i), \qquad (10)$$

where $\varepsilon_i{}^{(0)}$ is a concentration-independent term, V_i is the volume per cation i in the glass matrix, and γ_i is the activity of cation i. The average diffusion velocity of cation i, $\bar{v}_i$, in a homogeneous and isotropic medium due to a gradient in the chemical potential is given by

$$\bar{v}_i = -a_i \nabla \varepsilon_i, \qquad (11)$$

where a_i is a generalized mobility term. Thus the flux of cation i, $\bar{J}_i$, due to a gradient in the chemical potential becomes

$$\bar{J}_i = C_0 c_i \bar{v}_i = -a_i RT C_0 (\nabla c_i) \xi_i, \qquad (12)$$

where

$$\xi_i \equiv 1 + \frac{d \ln \gamma_i}{d \ln c_i}. \qquad (13)$$

In general, $\bar{v}_{Ag} \neq \bar{v}_{Na}$ leads to the creation of a space charge and an internal electric field, $\bar{E}_{int}$. Thus Eq. (12) must be modified to include a term for electric-field-induced drift as

$$\bar{J}_i = -D_i * \xi_i C_0 \nabla c_i + e \bar{E}_{int} u_i C_0 c_i, \qquad (14)$$

where e is the charge on an electron, μ_i is the mobility of cation i associated with electric-field-induced drift, and the self-diffusion coefficient is defined as

$$D_i * \equiv a_i RT. \qquad (15)$$

Assuming that no net current flows in the glass and that the Ag–Na exchange is a one-to-one exchange, i.e.,

$$\bar{J}_{Ag} + \bar{J}_{Na} = 0, \qquad (16)$$

$$c_{Ag} + c_{Na} = 1, \qquad (17)$$

respectively, Eqs. (14) and (16) may be combined to yield

$$\bar{E}_{\text{int}} = \frac{(D_{Ag}*\xi_{Ag} - D_{Na}*\xi_{Na})}{e(\mu_{Ag}c_{Ag} + \mu_{Na}c_{Na})} \; \nabla c_{Ag}. \qquad (18)$$

Equations (14) and (18) can be used together with the continuity equation

$$\frac{d(C_0 c_i)}{dt} = -\nabla \cdot \bar{J}_i \qquad (19)$$

to conclude

$$\frac{dc_{Ag}}{dt} = \nabla \cdot (D_{Ag}*\xi_{Ag}\nabla c_{Ag})$$
$$+ \nabla \cdot \left[\mu_{Ag} c_{Ag}\left(\frac{D_{Na}*\xi_{Na} - D_{Ag}*\xi_{Ag}}{\mu_{Ag} c_{Ag} + \mu_{Na}c_{Na}}\right) \nabla c_{Ag}\right]. \qquad (20)$$

For interstitial diffusion, the self-diffusion coefficient and the electric-field-induced mobility are related by the Nernst–Einstein relationship[8]:

$$D_i* = \frac{kT}{e} \; \mu_i. \qquad (21)$$

Ion exchange in glass, however, is not an interstitial process since it involves the exchange of ion species at fixed lattice sites. Thus Eq. (21) must be modified and the following semiempirical relationship is generally used[8,43]:

$$D_i* = H_i \frac{kT}{e}\mu_i, \qquad (22)$$

where H_i is known as the Haven ratio, which is a glass-dependent constant. The value of H_i typically lies between 0.3 and 1. From the Gibbs–Duhem equation of thermodynamics,[8]

$$\xi_{Ag} = \xi_{Na}. \qquad (23)$$

Combining Eqs. (17), (20), (22), and (23) with the assumption that

$$H_{Ag} = H_{Na}, \qquad (24)$$

we obtain

$$\frac{dc_{Ag}}{dt} = \nabla \cdot (\tilde{D} \nabla c_{Ag}), \qquad (25)$$

where the concentration-dependent interdiffusion coefficient $\tilde{D}$ is given by

$$\tilde{D} = \frac{D_{Ag}*D_{Na}*}{D_{Ag}*c_{Ag} + D_{Na}*c_{Na}} \left(1 + \frac{d \ln \gamma_{Ag}}{d \ln c_{Ag}}\right). \qquad (26)$$

Although Eq. (26) is widely quoted and used, the predictions of this equation have not always been consistent with observations.[10,44–46] Fortunately, the accurate modeling of the silver thermal ion exchange process is not dependent on the validity of Eq. (26) since $\tilde{D}$ can be obtained experimentally using the Boltzmann–Mantano inversion procedure described in Subsection 2.C.

In the limit of very low concentrations (i.e., $c_{Ag} \ll 1$ or $c_{Na} \ll 1$) of the indiffused cation (Ag or Na, respectively), ideal solution theory predicts that the bracketed thermodynamic term in Eq. (26) should be one.[8] Thus under such conditions the interdiffusion coefficient reduces to a self-diffusion coefficient, either $D_{Ag}*$ or $D_{Na}*$. Furthermore these self-diffusion coefficients can be measured using radiotracer studies.[44] Because of the mixed alkali effect, the self-diffusion coefficients are generally strongly concentration dependent.[47]

Device engineers often assume that $c_{Ag} \approx 0$ or at the very least that the self-diffusion coefficients are concentration independent, although both of these assumptions are often untrue in practice. For example, a 1 mol.% AgNO$_3$:99 mol.% NaNO$_3$ melt at 320 °C corresponds to a normalized silver concentration $c_{Ag}(0)$ in IEG of approximately 50%. And as indicated in Fig. 6, the interdiffusion coefficient of IEG varies by nearly a factor of 4 over the range $0 \leq c_{Ag} \leq 0.5$.

We have investigated the concentration dependence of the self-diffusion coefficients in IEG glass. Long-duration silver ion exchanges were performed in IEG using AgNO$_3$:NaNO$_3$ melts of two different concentrations. By measuring the surface refractive indices at 658 nm of these ion-exchanged samples with a RNF profilometer, we were able to deduce that 35% of the Na in the virgin glass had been replaced (in a top glass layer of thickness exceeding 80 μm) by Ag in the first sample and 85% in the second. A drop of radioactive tracers, drawn from liquid solutions of either Ag-108m or Na-22, was deposited on the glass surface of a virgin piece of IEG and on the surfaces of two previously exchanged pieces and allowed to dry. Each sample was then covered by a second identical piece of glass, effectively sandwiching the radioactive tracer between the pair. The radioactive tracers were thermally indiffused into the glass pair at 320 °C with the durations varying from 30 min to 1 h. Layer-by-layer etching of the glass using diluted hydrofluoric acid, followed by NaI well counting of the activity in the resultant etchant solution, allowed the indiffused radiotracer profiles to be measured.[10] Given the very low quantities of radiotracers used, it may be assumed that the entire quantity of radiotracer enters the glass nearly instantaneously. Under this condition, Eq. (2) may be solved in closed form for the
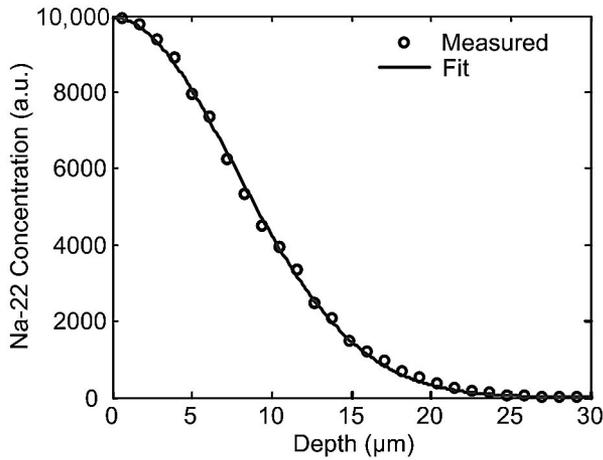
Fig. 7. Na-22 diffusion profile in IEG glass sample 3 with 85% of the Na in the virgin glass replaced by Ag. The diffusion was performed at 320 °C for 60 min.

concentration profile $c_i(x, t)$ of the indiffused radioactive tracers. The solution is a Gaussian function of depth as given by Eq. (27):

$$c_i(x, t) = \frac{c_0^{(i)}}{\sqrt{\pi D_i^* t}} \exp\left(-\frac{x^2}{4D_i^* t}\right), \qquad (27)$$

where t is the diffusion duration, $c_0^{(i)}$ is a constant, and i denotes either Ag or Na. Note that Eq. (27) satisfies the necessary boundary conditions:

$$c_i \to 0 \text{ as } t \to \infty, \text{ for } x > 0,$$

$$c_i \to \infty \text{ as } t \to 0, \text{ for } x = 0,$$

$$\int_0^\infty c_i(x, t)\mathrm{d}x = c_0^{(i)}, \text{ for all } t. \qquad (28)$$

The Gaussian dependence predicted by Eq. (27) was experimentally confirmed in IEG, and a particular result, for the case of Na-22 indiffusion, is shown in Fig. 7. The self-diffusion coefficients D_i^* for both Ag-108m and Na-22 were determined for three different glass compositions (i.e., 1, 2, and 3) by fitting the experimentally measured concentration profiles to the functional form given by Eq. (27), and the results are shown in Table 3. These results demonstrate that the self-diffusion coefficients are concentration dependent in IEG. In particular, the Ag self-diffusion coefficient D_{Ag}^* varies by nearly a factor

Table 3. Silver and Sodium Tracer Diffusion Coefficient at 320 °C

IEG Glass	D_{Ag} (10^{-15} m^2/s)	D_{Na} (10^{-15} m^2/s)
1: 100% Na (virgin glass)	5.2	7.0
2: 35% Na replaced by Ag	8.6	8.1
3: 85% Na replaced by Ag	24.1	7.5

of 5 as the relative Ag concentration in the glass increases from 0% to 85%. Similar results have been previously reported in other glasses.[10]

E. Dispersion

The refractive index of glass is known to be wavelength dependent. The refractive index n_{sub} of virgin IEG was measured at four different wavelengths using a commercial prism coupling instrument. The wavelength dependence of the refractive index change induced by ion exchange was also determined as described below.

The induced refractive index change is linearly proportional to the indiffused silver ion concentration as established in Figs. 4 and 5. This linear dependence can be expressed as

$$\Delta n(x) = \alpha(\lambda)c_{Ag}(x), \qquad (29)$$

where the constant of proportionality α is wavelength dependent. To determine $\alpha(\lambda)$, a planar waveguide was fabricated in 1 mol.%. Ag nitrate melt at 320 °C for 4 h. The resulting refractive index profile was measured using a RNF profilometer operating at 658 nm, and the corresponding indiffused relative silver ion concentration $c_{Ag}(x)$ was computed from this data using the linear relationship given in Fig. 4. The effective indices of the guided planar TE waveguide modes were measured at four different wavelengths, 632.8, 830, 1300, and 1550 nm, using a prism coupler. A finite-difference method (FDM) was implemented to solve Maxwell's equations for the effective indices of the TE planar waveguide modes given a refractive index profile and a specified wavelength. Using the FDM effective index solver together with the known silver ion concentration profile, an iterative search was implemented to find values of α for each of the four wavelengths that produced good fits between the measured and com-
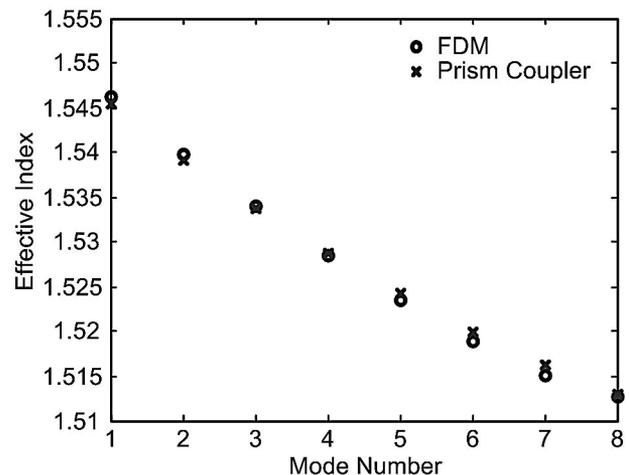

Fig. 8. Effective indices of planar waveguide fabricated in 1 mol.% AgNO$_3$ at 320 °C for 4 h comparison of the prism coupler measured data with FDM-calculated data at 1.55 μm with α = 0.847.

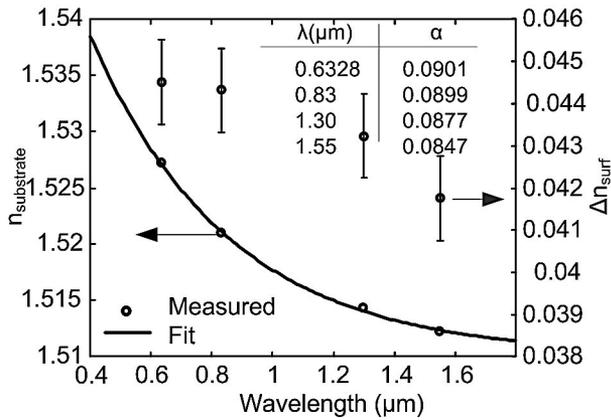Fig. 9. Dispersion of IEG substrate and ion-exchanged planar waveguide fabricated at 320 °C for 4 h using 1 mol.% AgNO$_3$.

Fig. 10. Comparison of the modeled diffusion profile with the experimental results for planar waveguides.

puted effective indices. A typical result is shown in Fig. 8 for λ equal to 1550 nm. The wavelength dependencies of both the bulk refractive index and the induced index changes are shown in Fig. 9. The measurement accuracies of both the commercial prism coupler and the commercial RNF profilometer are reported to be no better than ± 0.001. Thus the error bars for the dispersion of the refractive index change shown in Fig. 9 are quite large. Nonetheless, we are able to conclude that the dispersion of the refractive index change is less than 10% over the wavelength band spanning 633 to 1550 nm.

3. Modeling Results

A. Planar Waveguides

The accuracy of the model described in Section 2 was evaluated for planar and channel waveguides fabricated under a variety of conditions. Equation (2) was solved, using the data given in Fig. 6, to predict the induced refractive index and/or silver ion concentration profile.

The following boundary conditions were assumed:

$$c_{Ag} = c_{surf} \text{ at } x = 0 \text{ for all } t,$$

$$c_{Ag} = 0 \text{ for } x > 0 \text{ at } t = 0, \qquad (30)$$

where the value of c_{surf}, the relative Ag cation concentration at equilibrium immediately inside the glass surface, depends on the melt concentration as described in Subsection 2.B.

Figure 10 shows a typical result for a planar waveguide fabricated by ion exchange using 1 mol.% AgNO$_3$ at 320 °C for 4 h followed by a subsequent thermal anneal, with no melt present, performed for two additional hours at 320 °C. The Ag concentration profile in the glass was measured by the BSE method and compared with the profiles predicted by the numerical solution of Eq. (2) obtained using the FDM. As indicated by Fig. 10, the agreement between the measurement and theory is excellent.
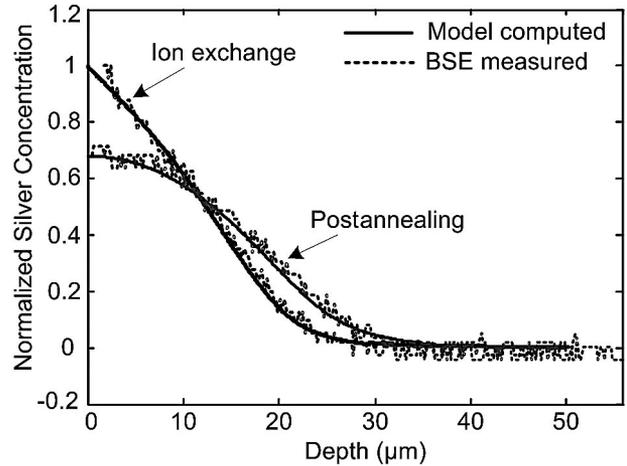
As mentioned above, device engineers often as-

sume that the interdiffusion coefficient $\tilde{D}$ is concentration independent. Under such an assumption, Eq. (2) can be solved in closed form for a planar waveguide to yield

$$c_{Ag}(x, \ t) = c_{surf} \ \text{erfc}\big(x/2\sqrt{\tilde{D}t}\big), \qquad (31)$$

where the function erfc(z) is defined as

$$\text{erfc}(z) \equiv \frac{2}{\sqrt{\pi}} \int_z^\infty \exp(-t^2)\mathrm{d}t. \qquad (32)$$

It is clear from Fig. 6, however, that the interdiffusion coefficient is strongly concentration dependent for the planar waveguide studied in Fig. 10, since c_{Ag} varies from 0.5 at the glass surface to 0 at a depth of ~30 μm. Thus, as expected, empirical attempts to fit Eq. (31) to the measured data (i.e., measured BSE without anneal) have been unsuccessful. The errors associated with such a fit are large, as compared with the results in Fig. 10.

B. Channel Waveguides

Channel waveguides were fabricated using a 30 min thermal silver ion exchange through 3–7 μm wide mask openings with a 1 mol.% AgNO$_3$ melt at 320 °C. The mask consisted of 150 nm of E-beam evaporated titanium that was subsequently chemically etched to define the diffusion openings. The mask was chemically anodized in a NaNO$_3$ salt bath at 330 °C for 1 h before the ion exchange was performed. This step was implemented to reduce the clustering of Ag ions that often occurs at the edges of the mask openings and leads to high propagation losses. The resulting two-dimensional (2-D) refractive index profiles $\Delta n(x, y)$ were measured at 658 nm using the RNF profilometer (x is the depth measured from the glass surface and y is the lateral displacement measured from the center of the diffusion mask opening). Figure 11
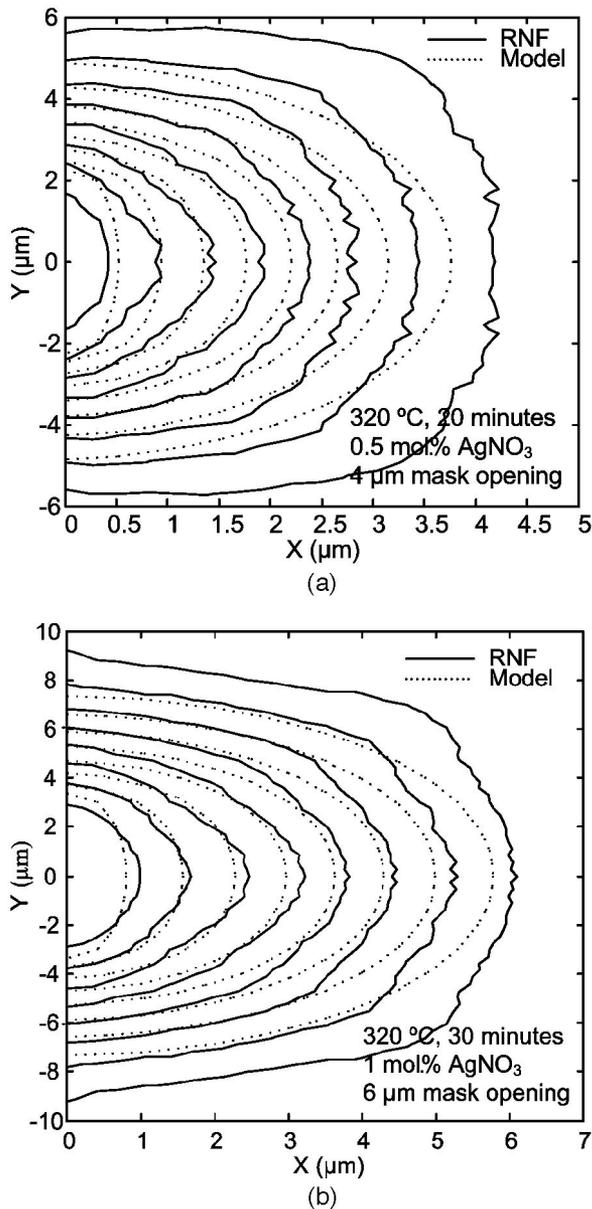
(a)

(b)

Fig. 11. Comparison of the computed diffusion profile with measured results for channel waveguides fabricated under different conditions. The inner contours in each of the two graphs correspond to $\Delta n = 0.9\Delta n_{surf}$, while each succeeding contour line represents an additional change of the refractive index in decrements of $0.1\Delta n_{surf}$.

shows the comparison of the RNF-measured $\Delta n(x, y)$ with the model predictions obtained by numerically solving Eq. (2) using the measured interdiffusion coefficient shown in Fig. 6 and the following boundary conditions:

$$c_{Ag} = c_{surf} \text{ at } x = 0, \ |y| \leq w, \ t \geq 0,$$
$$c_{Ag} = 0 \text{ for } x > 0, \ t = 0, \text{ and all } y,$$
$$\left.\frac{\partial c_{Ag}}{\partial x}\right|_{x=0} = 0 \text{ for } |y| > w, \ t \geq 0, \quad (33)$$

where w is the width of the mask opening. The agree-

ment between the measured profile and that predicted by the model, with no free parameters, is reasonably good. As can be seen in Fig. 11, the largest discrepancies occur in the regions of low concentration and close to the glass surface. It is possible that these discrepancies are due to the presence of the oxidized metal mask, which may introduce an electric field generated by the electrochemical bias between the melt and the mask.[48] This field may alter the diffusion process in some small but subtle ways. It would be interesting to repeat these experiments using dielectric rather than metal masks.

4. Optical Device Performance

The procedure described above for studying the ion exchange process in IEG glass is, in general, applicable to other single-alkali glasses. The n and K values in the equilibrium relation, the self-diffusion and interdiffusion coefficients, and $\alpha(\lambda)$ will depend, however, on the glass composition. Once these parameters are measured and the fabrication conditions specified, the model described in the previous sections can be used to determine the induced refractive index profile at a particular operating wavelength. Finally, standard techniques, such as the beam propagation method, FDM, CMT, finite-difference time-domain, etc., can be used to determine the optical characteristics of a waveguide device from knowledge of its refractive index profiles. In this section we illustrate this final optical modeling step.

A series of integrated optic ring resonators were fabricated in IOG10 by conventional photolithography and thermal silver ion exchange.[49] A 150 nm thick layer of titanium was E-beam deposited on an IOG10 glass substrate. Using standard photolithography, a pattern of diffusion openings was created in the titanium layer corresponding to a set of ring resonators. The mask was anodized at 330 °C in a pure $NaNO_3$ melt for 1 h to mitigate the effects of Ag clustering as described earlier. Next, ion exchange was performed in a mixed melt of 0.6 mol.% $AgNO_3$ and 99.4 mol.% $NaNO_3$ at 320 °C for 20 min. Following the exchange, the wafer was removed from the oven and allowed to cool to room temperature, and the individual resonator chips were diced out of the full wafer and polished.

Ideally, in terms of continuity with Sections 1–3, the ring resonators would have been fabricated in IEG substrates. Unfortunately, however, to obtain good optical quality (i.e., no bubbles and very low striae), high-silica glasses must be melted at high temperatures in large batches. The cost of melting such a large batch of glass for scientific purposes is prohibitive. Mixed-alkali glasses are common and have been developed for a host of unrelated applications; thus most waveguide devices fabricated by ion exchange have been produced in these glasses solely because they are readily available. If commercial demand was sufficiently high, as it was during the telecommunications bubble, then single-alkali glasses would be readily available too. In fact, Schott Glass Technologies did at one time develop such a glass,
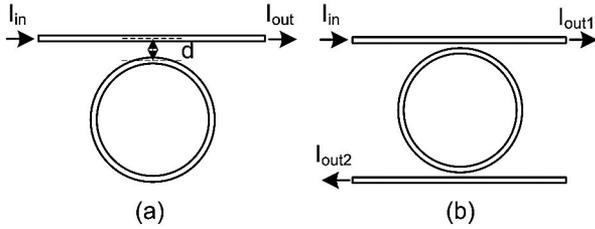
Fig. 12. Illustration of the ring resonators: (a) single-arm ring resonator, (b) dual-arm ring resonator.

Fig. 13. Photograph of a dual-arm ring resonator illuminated at 632.8 nm.

BGG31, that was used by IOT in Germany to make glass-integrated optical devices.[22,23] Our IEG glass melt was of small volume, and consequently it had lower optical quality than commercially available mixed-alkali glasses like IOG10. IOG10 contains both Na_2O and K_2O, and therefore we made no attempt to model the ion exchange diffusion process in this mixed-alkali glass. For our immediate optical modeling purposes, however, the inability to perform this task does not present any difficulties. We have already demonstrated in Sections 1–3 that refractive index profiles can be accurately predicted based on Fickian diffusion theory in a single-alkali glass without invoking free parameters. Thus it only remains to show that device operation can be predicted accurately in a glass (composition unimportant) once the refractive index profile is known. Although this type of work is routinely reported for step-index waveguides, such as those produced using silica-on-silicon technology, similar results have not been presented for diffused waveguides with graded refractive index profiles. The lack of such results is primarily due to the difficulties inherent in accurately measuring 2-D refractive index profiles. Recently, however, RNF profilometers have become commercially available, thus making such measurements possible. In this section we demonstrate that we can accurately predict the operation of an ion-exchanged ring resonator device once the refractive index profile is known. We accomplish this task in a commercially available mixed-alkali glass, which is similar in composition to IEG. The refractive index profile, however, is directly measured using a RNF profilometer rather than computed using Fickian diffusion theory. We also note that the devices reported in this section are, to the best of our knowledge, as good as or better than (i.e., in terms of low loss—0.1 dB/cm) anything previously reported by thermal silver ion exchange in glass. Thus these devices are of some interest in their own right.

Each resonator consisted of a ring and directional coupler(s) as illustrated in Fig. 12 for single- and dual-arm devices, respectively. In these devices, all the waveguides were observed to be single moded at operating wavelengths in the vicinity of 1550 nm. A set of single-arm resonators, identical in all respects except for the variation of center-to-center separation d between the straight waveguide and the ring, were fabricated an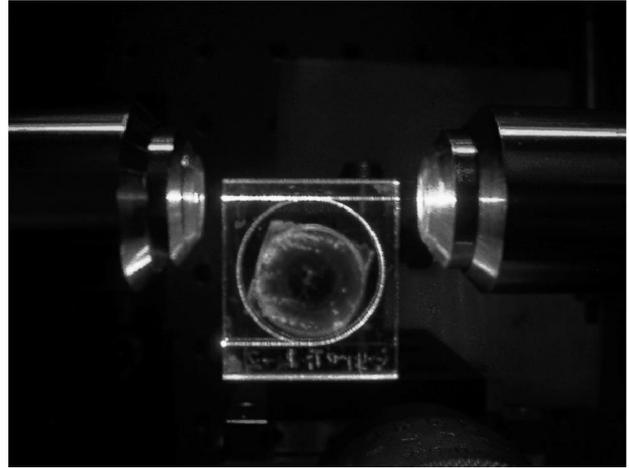d evaluated. The mask openings for both the straight waveguides and the 1.6 cm diameter ring were fixed at a width of 2 μm.

The transmittance of a single-arm ring resonator is given by[50]

$$T_r(\phi) \equiv \frac{I_{out}}{I_{in}} = \left| (1-\Gamma)^{1/2} \frac{y - x\exp(-j\phi)}{1 - xy\exp(-j\phi)} \right|^2, \quad (34)$$

$$x \equiv (1-\Gamma)^{1/2}\exp(-\alpha L/2)$$
$$= \exp\left\{ -\left[\alpha - \frac{\ln(1-\Gamma)}{L} \right] L/2 \right\}, \quad (35)$$

$$y \equiv \sqrt{1 - K_c}, \quad (36)$$

$$\phi = \frac{2\pi}{\lambda} N_{eff} L, \quad (37)$$

where I_{in} and I_{out} are the optical powers measured at the input and output ports, respectively; Γ is the power insertion loss coefficient of the directional coupler; K_c is the power crossover efficiency of the directional coupler; α is the power propagation loss coefficient in the ring; L is the circumference of the ring; N_{eff} is the effective index of the waveguide mode; λ is the operating wavelength; and ϕ is the round-trip phase change accumulated by an optical beam as it propagates once around the ring. The finesse F and dip D_p of a single-arm resonator may be easily computed from Eqs. (34)–(37) to yield

$$F \equiv \frac{2\pi}{\Delta\phi_{FWHM}} = \frac{\pi}{\cos^{-1}\left(\frac{2xy}{1 + x^2 y^2} \right)}, \quad (38)$$

$$D_p \equiv \frac{T_{max} - T_{min}}{T_{max}} = \frac{4xy(1 + x^2 y^2 - x^2 - y^2)}{(1 - xy)^2(x + y)^2}, \quad (39)$$

where $\Delta\phi_{FWHM}$ is the full width at half-maximum of the spectral transmittance dip.

The spectral response of each resonator was characterized by using a narrow linewidth, external-cavity tunable diode laser source operating in the vicinity of 1550 nm. As illustrated in Fig. 13, the laser beam was end-fired coupled into the input port of the ring resonator using a $20\times$ micro-objective lens. The fraction of incident light transmitted through to the output port was collected using a $20\times$ objective lens and measured by a photodiode detector as the laser wavelength was tuned over a small range in the vicinity of 1550 nm. From the measured spectral response, the finesse and dip could be determined, then the effective loss coefficient $\alpha - [\ln(1 - \Gamma)]/L$ and crossover efficiency K_c were derived using Eqs. (35), (36), (38), and (39). The effective losses of the resonators were originally ~1 dB/cm, which is quite high.

To reduce the losses, the devices were thermally annealed at 320 °C in 10 min steps. After each annealing step, the finesse and dip of the resonators were remeasured and the crossover efficiencies and effective losses were recomputed. The losses initially decreased with each additional thermal anneal step, until the confinement of the waveguide mode was sufficiently weak so that bending losses began to become significant. Table 4 gives the coupler's crossover efficiency and the effective loss following each annealing step corresponding to a directional coupler spacing of 10.5 μm. Note that the device achieved its minimum loss after the sixth annealing step. Similar data were collected for the resonators with other coupler spacings. A new set of devices was fabricated; for each device, thermal annealing was halted at the previously determined step (i.e., sixth) of minimum loss. The waveguide refractive index profiles of these minimum loss devices were also measured using a RNF profilometer. Figures 14(a) and 15 show the spectral response and refractive index profile, respectively, obtained for a typical minimum loss device. The measured finesse and dip of this device were 37 and 80%, respectively, corresponding to an effective loss of 0.1 dB/cm and a coupler crossover efficiency of 4.6%. Similar results for a dual-arm ring resonator, as shown in Fig. 14(b), were obtained with a finesse of 40, and dip of 44%, corresponding to an effective loss of 0.1 dB/cm and a coupler crossover efficiency of 1.7%.
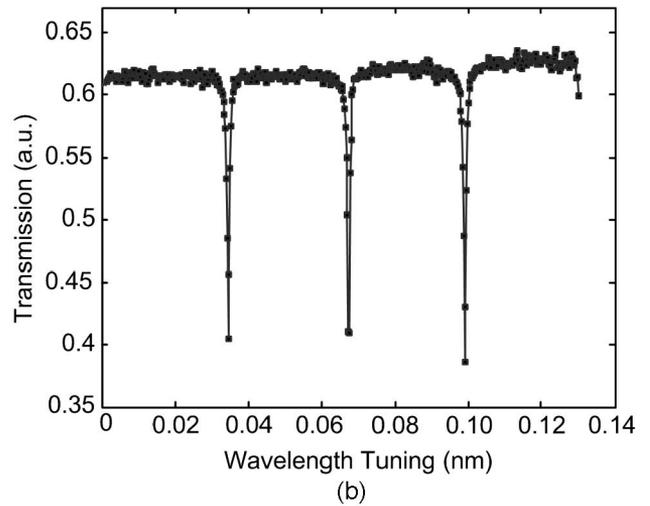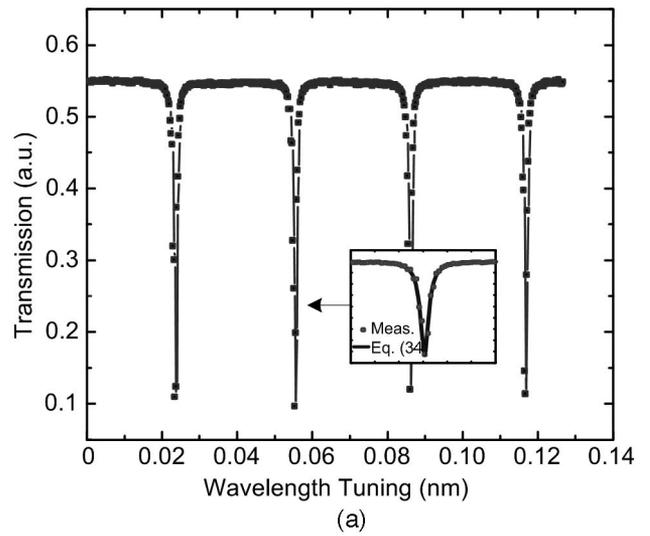

(a)

(b)

Fig. 14. Measured spectral response of ring resonators with a 1.6 cm diameter: (a) single-arm ring resonator with center-to-center coupler spacing of 10.5 μm, (b) dual-arm ring resonator with center-to-center coupler spacing of 11.5 μm.

Using the FDM, the mode profile of the minimum loss waveguides was computed from the measured

Table 4. Waveguide Annealing Results for 1.6 cm Diameter Ring with a Coupler Waveguide Spacing of 10.5 μm

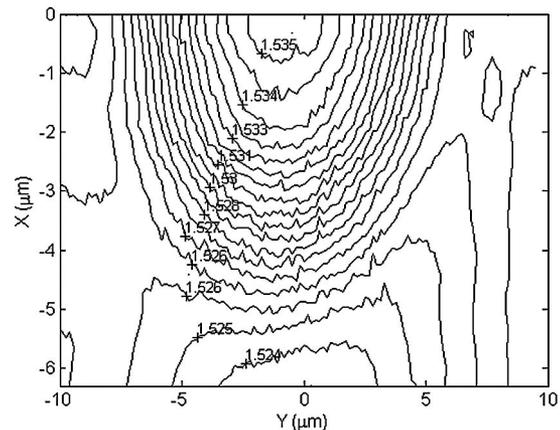| IOG10 Annealing Step	K_c (%)	α (dB/cm)
1	0.19	0.22
2	0.53	0.20
3	1.35	0.23
4	2.14	0.13
5	3.6	0.13
6	4.6	0.10
7	6.6	0.13

Fig. 15. RNF measurement of the channel waveguide index profile for a minimum loss device.
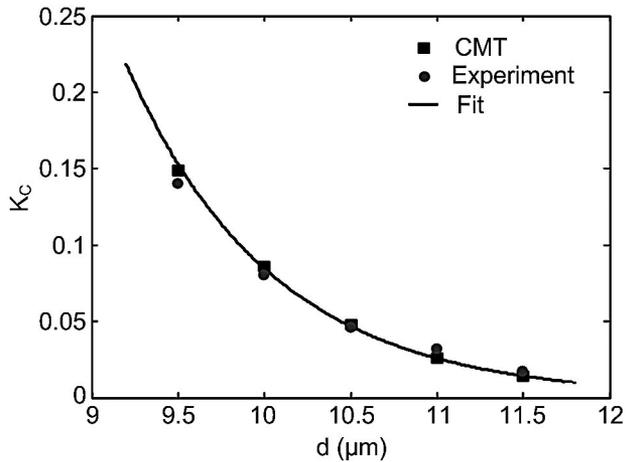
Fig. 16. Comparison of the measured and CMT-predicted coupling ratios.

refractive index profile. The spatial mode overlap integral between the straight waveguide mode and the identical ring waveguide mode was numerically evaluated at a sequence of closely spaced points along the coupler's length. From this data, the spatially vary-
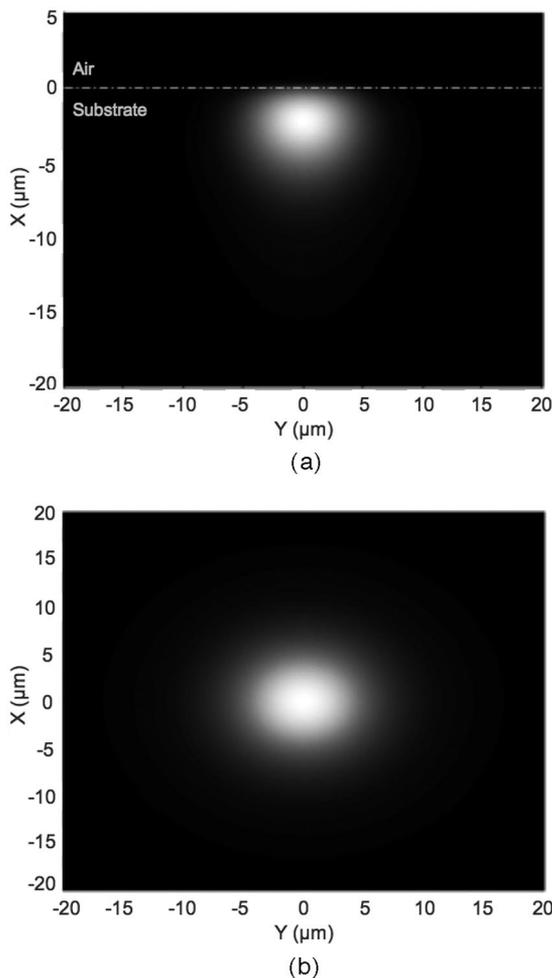

(a)

(b)

Fig. 17. Comparison of mode field profiles for (a) the waveguide shown in Fig. 15 and (b) a standard SMF-28 optical fiber.

ing coupling coefficient was determined. CMT was then used to compute the crossover efficiency K_c of the directional coupler.[51] The results were found to be in excellent agreement with measured values as shown in Fig. 16.

Figure 17 shows the waveguide mode profile corresponding to Fig. 15. Also shown in this figure is the mode profile of a standard SMF-28 optical fiber. On the basis of these two profiles, the fiber-to-waveguide insertion loss was computed to be ~1.5 dB based on a mode overlap integral.

5. Conclusions

In conclusion, we have demonstrated that the induced refractive index distribution in a channel waveguide, fabricated by thermal silver ion exchange in a single-alkali glass, can be predicted from a model based on first principles. Furthermore, the parameters used in the model can be measured directly and need not be inferred by making assumptions whose validity is questionable. Once the refractive index profile is known, we have also demonstrated that standard numerical techniques may also be used to accurately determine the optical characteristics of functional devices. The techniques described here provide a systematic methodology for the design and fabrication of glass integrated optic devices using thermal silver ion exchange.

References

1. T. Izawa and H. Nakagome, "Silver ion-exchanged glass waveguides," Appl. Phys. Lett. **21,** 584–586 (1972).
2. S. I. Najafi, ed., *Introduction to Glass Integrated Optics* (Artech, 1992).
3. T. Findakly, "Glass waveguides by ion exchange: a review," Opt. Eng. **24,** 244–250 (1985).
4. R. V. Ramaswamy and R. Srivastava, "Recent advances in ion-exchanged optical waveguides and components," J. Mod. Opt. **35,** 1049–1067 (1988).
5. R. V. Ramaswamy and R. Srivastava, "Ion-exchanged glass waveguides: a review," J. Lightwave Technol. **6,** 984–1001 (1988).
6. H. M. Garfinkel, "Ion-exchange equilibria between glass and molten salts," J. Phys. Chem. **72,** 4175–4181 (1968).
7. R. H. Doremus, "Exchange and diffusion of ions in glass," J. Phys. Chem. **68,** 2212–2218 (1964).
8. P. Shewmon, *Diffusion in Solids,* 2nd ed. (The Minerals, Metals and Materials Society, 1989).
9. R. H. Doremus, *Glass Science,* 2nd ed. (Wiley, 1994), Chap. 15.
10. B. Messerschmidt, C. H. Hsieh, B. L. McIntyre, and S. N. Houde-Walter, "Ionic mobility in an ion exchanged silver-sodium boroaluminosilicate glass for micro-optics applications," J. Non-Cryst. Solids **217,** 264–271 (1997).
11. H. Wakabayashi, "The relationship between kinetic and thermodynamic properties in mixed alkali glass," J. Non-Cryst. Solids **203,** 274–279 (1996).
12. G. Stewart, C. A. Millar, P. J. R. Laybourn, C. D. W. Wilkinson, and R. M. DelaRue, "Planar optical waveguides formed by silver ion migration in glass," IEEE J. Quantum Electron. **QE-13,** 192–200 (1977).
13. G. Stewart and P. J. R. Laybourn, "Fabrication of ion-exchanged optical waveguide from diluted silver nitrate melts," IEEE J. Quantum Electron. **QE-14,** 930–934 (1978).
14. H.-J. Lilienhof, E. Voges, D. Ritter, and B. Pantschew, "Field-induced index profiles of multimode ion-exchanged strip

waveguides," IEEE J. Quantum Electron. **QE-18,** 1877–1883 (1982).

15. R. G. Walker, C. D. W. Wilkinson, and J. A. H. Wilkinson, "Integrated optical waveguiding structures made by silver ion-exchange in glass. 1: The propagation characteristics of stripe ion-exchanged waveguides: a theoretical and experimental investigation," Appl. Opt. **22,** 1923–1928 (1983).

16. R. Lagu and R. Ramaswamy, "Process and waveguide parameter relationships for planar silver ion-exchanged glass waveguides," J. Lightwave Technol. **LT-4,** 176–181 (1986).

17. R. V. Ramaswamy and S. I. Najafi, "Planar, buried, ion-exchanged glass waveguides: diffusion characteristics," IEEE J. Quantum Electron. **QE-22,** 883–891 (1986).

18. L. Roβ, N. Fabricius, and H. Öeste, "Single mode integrated optical waveguides by ion-exchange in glass," in *Proceedings of EFOC/LAN 87* (Information Gatekeepers, 1987), pp. 99–103.

19. R. V. Ramaswamy, R. Srivastava, P. Chludzinski, and J. T. Anderson, "Influence of Ag^+-Na^+ ion-exchange equilibrium on waveguide index profiles," IEEE J. Quantum Electron. **24,** 780–785 (1988).

20. R. V. Ramaswamy, H. C. Cheng, and R. Srivastava, "Process optimization of buried Ag^+-Na^+ ion-exchange waveguides: theory and experiment," Appl. Opt. **27,** 1814–1819 (1988).

21. S. Honkanen and A. Tervonen, "Experimental analysis of Ag^+-Na^+ exchange in glass with Ag film ion sources for planar optical waveguide fabrication," J. Appl. Phys. **63,** 634–639 (1988).

22. N. Fabricius, H. Öeste, H.-J. Guttmann, H. Quast, and L. Ross, "BGG 31: a new glass for multimode waveguide fabrication," in *Proceedings of EFOC/LAN 88* (Information Gatekeepers, 1988), pp. 59–62.

23. L. Roβ, "Integrated optical components in substrate glasses," Glastech Ber. **62,** 285–297 (1989).

24. H. C. Cheng and R. Ramaswamy, "Simulation of tapered transitions in ion-exchanged channel waveguides," Appl. Opt. **29,** 1150–1156 (1990).

25. J. Albert and J. W. Y. Lit, "Full modeling of field-assisted ion exchange for graded index buried channel optical waveguides," Appl. Opt. **29,** 2798–2804 (1990).

26. M. C. Page, R. Oven, and D. G. Ashworth, "Scaling rules for glass based planar optical waveguides made by field assisted ion diffusion," Electron. Lett. **27,** 2073–2076 (1991).

27. T. Poszner, G. Schreiter, and R. Muller, "Stripe waveguides with matched refractive index profiles fabricated by ion exchange in glass," J. Appl. Phys. **70,** 1966–1974 (1991).

28. J. Johansson, G. Djanta, and J.-L. Coutaz, "Optical waveguides fabricated by ion exchange in high-index commercial glasses," Appl. Opt. **31,** 2796–2799 (1992).

29. I. G. Voitrnko, V. P. Reko, L. I. Sotskaya, and A. V. Tomov, "Mode interference pattern in ion-exchanged channel waveguides," in Proc. SPIE **1932,** 2–13 (1993).

30. B. Pantchev and Z. Nikolov, "Characterization of refractive index profiles in silver-sodium ion-exchanged glass waveguides for homogeneous refracting waveguide structures," IEEE J. Quantum Electron. **29,** 2459–2465 (1993).

31. D. G. Ashworth, R. Oven, and M. C. Page, "The influence of the pseudo-mixed-alkali effect on the field-assisted diffusion of

silver ions into glass for optical waveguides," J. Phys. D **28,** 657–664 (1995).

32. A. Lupascu, A. Kevorkian, T. Boudet, F. Saint-Andre, D. Persegol, and M. Levy, "Modeling ion exchange in glass with concentration-dependent diffusion coefficients and mobilities," Opt. Eng. **35,** 1603–1610 (1996).

33. A. Lupascu, A. Kevorkian, C. P. Cristescu, and I. M. Popescu, "Local electric fields in optical glasses during field-assisted ionic exchanges," in Proc. SPIE **4068,** 26–32 (2000).

34. J.-E. Broquin, "Ion exchanged integrated devices," in Proc. SPIE **4277,** 105–117 (2001).

35. P. Y. Choo, J. A. Frantz, J. T. A. Carriere, D. L. Mathine, R. K. Kostuk, and N. Peyghambarian, "Measurement and modeling of ion-exchange parameters for IOG-10 glass," Opt. Eng. **42,** 2812–2816 (2003).

36. A. Bradenburg, "Stress in ion-exchanged glass waveguides," J. Lightwave Technol. **LT-4,** 1580–1593 (1986).

37. C. De Bernardi, S. Morasca, D. Scarano, A. Camera, and M. Morra, "Compositional and stress-optical effects in glass waveguides: comparison between K-Na and Ag-Na ion exchange," J. Non-Cryst. Solids **119,** 195–204 (1990).

38. R. Araujo, "Colorless glasses containing, ion-exchanged sliver," Appl. Opt. **31,** 5221–5224 (1992).

39. C. Kaps and W. Fliegel, "Sodium/silver ion exchange between a non-bridging oxygen-free boroaluminosilicate glass and nitrate melts," Glastech. Ber. **64,** 199–204 (1991).

40. R. W. Laity, "Fused salt concentration cells with transference. Activity coefficients in the system silver nitrate-sodium nitrate," J. Am. Chem. Soc. **79,** 1849–1851 (1957).

41. R. Goring and M. Rothhardt, "Application of the refracted near-field technique to multimode planar and channel waveguides in glass," J. Opt. Commun. **7,** 82–85 (1986).

42. J. Crank, *The Mathematics of Diffusion* (Clarendon, 1976), Chap. 7.

43. W. Beier and G. H. Frischat, "Transport mechanisms in alkali silicate glasses," J. Non-Cryst. Solids **73,** 113–133 (1985).

44. S. A. Poling and S. N. Houde-Walter, "Structural factors in silver-induced relaxation in aluminosilicate glasses," J. Non-Cryst. Solids **293–295,** 430–439 (2001).

45. R. Terai, H. Wakabayashi, and H. Yamanaka, "Haven ratio in mixed alkali glass," J. Non-Cryst. Solids **103,** 137–142 (1988).

46. H. Wakabayashi, "The relationship between kinetic and thermodynamic properties in mixed alkali glass," J. Non-Cryst. Solids **203,** 274–279 (1996).

47. D. E. Day, "Mixed alkali glasses—their properties and uses," J. Non-Cryst. Solids **21,** 343–372 (1976).

48. G. Chartier, P. Collier, A. Guez, P. Jaussaud, and Y. Won, "Graded-index surface or buried waveguides by ion exchange in glass," Appl. Opt. **19,** 1092–1095 (1980).

49. G. Li and K. A. Winick, "Integrated optical ring resonators fabricated by silver ion exchange in glass," in *Conference on Lasers & Electro-Optics* (Optical Society of America, 2004), paper CWA63.

50. K. Okamoto, *Fundamentals of Optical Waveguides* (Academic, 2000), Chap. 4.

51. T. Tamir, ed., *Guided-Wave Optoelectronics* (Springer-Verlag, 1988), Chap. 2.